2025 International Conference on Metaverse Computing, Networking and Applications (MetaCom) | 979-8-3315-2255-1/25/$31.00 ©2025 IEEE | DOI: 10.1109/MetaCom65502.2025.00040

Offline Modeling and Mixed Reality Based Remote Diagnosis System for Patient-Specific Cardiovascular Diseases

Jing-Yuan Wang
University of Macau
Macau, China
yc27479@um.edu.mo

Yujie Gong
University of Macau
Macau, China
yc17470@um.edu.mo

Yuxin Shan
Chinese Academy of Sciences
Shenzhen, Guangdong, China
yx.shan@siat.ac.cn

Fenfen Qi
University of Macau
Macau, China
yc27956@um.edu.mo

Yingzhi Liu
University of Macau
Macau, China
yingzhiliu@um.edu.mo

Zhengzheng Yan
Chinese Academy of Sciences
Shenzhen, Guangdong, China
zz.yan@siat.ac.cn

Zaiheng Cheng
Chinese Academy of Sciences
Shenzhen, Guangdong, China
zh.cheng@siat.ac.cn

Rongliang Chen
Chinese Academy of Sciences
Shenzhen, Guangdong, China
rl.chen@siat.ac.cn

Xinhong Wang
The Second Affiliated Hospital
Zhejiang University School of Medicine
Hangzhou, Zhejiang, China
2611104@zju.edu.cn

Li Luo
University of Macau
Macau, China
liluo@um.edu.mo

Xiao-Chuan Cai
University of Macau
Macau, China
xccai@um.edu.mo

***Abstract*—This paper presents a mixed reality (MR) based, high-performance-computing supported, remotely connected collaborative platform for the diagnosis of and the surgical planning for cardiovascular diseases. Recognizing the fact that the human cardiovascular system is an interconnected network where pathological alterations in one organ (e.g., the heart) may critically impact the others (e.g., the brain), our study emphasizes the multi-organ hemodynamic coupling for the purpose of surgical planning. The system combines offline numerical modeling and MR-guided online collaboration, i.e., physics based simulations of hemodynamics involving multiple organs using patient-specific vascular geometry reconstructed from computed tomography (CT) or magnetic resonance imaging (MRI) images, high resolution numerical modeling, and a remote interface allowing doctors to interactively view and modify 3D holograms of a cardiovascular network and numerical simulation results with hand gestures or voice commands via head-mount displays. As an example, we investigate the perioperative ischemic stroke risk during a coronary revascularization procedure. The study shows how a stent-induced coronary geometry change propagates hemodynamic perturbations to the cerebral vascular, validates through synchronized multi-experts exploration of the virtual anatomy. By unifying high performance computing, multi-organ coupled numerical simulation, geographically distributed MR collaboration, and an interactive visualization, this system provides a diagnosis and surgical planning platform with a precision and convenience beyond existing approaches in medical practices.**

***Index Terms*—Remote collaboration diagnosis, holographic device interaction, offline simulation, computational hemodynamics, cardio-cerebral coupling high-performance parallel computing**

The research is supported by NSFC 12371442 and FDCT 0035/2025/RIA1, 0146/2024/RIA2, 0090/2022/A2, 0079/2021/AFJ, 0141/2020/A3. L. Luo and X.-C. Cai are the corresponding authors of the paper.

I. Introduction

Cardiovascular diseases (CVDs) pose a significant threat to global health due to their high mortality and morbidity rates, as well as their wide range of harmful effects on the body. Among these, coronary artery disease (CAD) is particularly common and dangerous, characterized by arterial blockages that restrict blood supply to the heart muscle, CAD is a leading cause of mortality worldwide. Coronary stenting plays a crucial role in treating related conditions, aiming to enhance myocardial blood flow and reduce ischemic risks by altering the shape of blood vessels. However, the cardiovascular system functions as an integrated network (see Figure 1), meaning localized treatments can overlook broader hemodynamic impacts. For example, valve replacement may reduce cardiac output, leading to diminished renal blood flow. Similarly, changes in coronary anatomy during revascularization may disrupt cerebral blood flow, potentially causing life-threatening perioperative ischemic strokes. Therefore, it's essential to evaluate the clinical approaches from a holistic perspective, considering the entire cardiovascular system and potential impacts on cerebral blood flow. This comprehensive analysis can improve surgical outcomes by addressing the interconnected risks inherent to CVD management.

Numerical simulations offer a non-invasive way to assess these systemic interactions, providing critical insights into hemodynamic variables and morphological changes. Significant progress has been made in modeling single-organ systems, such as the coronary arteries [1] or cerebral vascular [2],

979-8-3315-2255-1/25/$31.00 ©2025 IEEE
DOI 10.1109/MetaCom65502.2025.00040

[3], these studies cannot capture multi-organ responses. For instance, they may not predict how coronary stent placement affects cerebral blood flow, limiting their utility in predicting surgical risks. The cardio-cerebral network (including

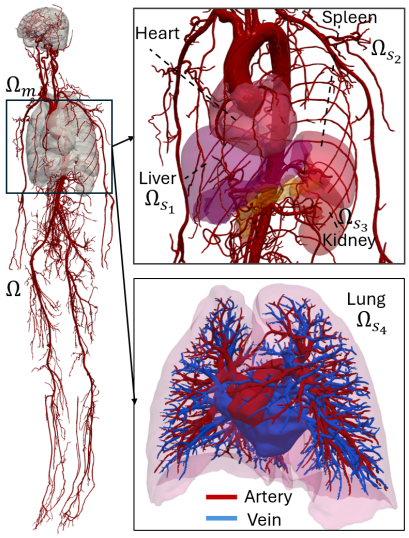

Fig. 1. Human arterial network. The global domain Ω consists of major arteries Ω_m and organ-specific vascular subnetworks (Ω_{s_i}, $i = 0, \ldots, n_s$), n_s is the number of coupled organs.

coronary arteries, aortic arch, carotid arteries, and cerebral vessels) presents unique computational challenges, its complex morphology (stenoses, bifurcations, and submillimeter vessels) requires high-resolution meshes and patient-specific boundary conditions to resolve transient flow phenomena. To date, only Yan et al. [4] have explored this interconnected system. This study focuses on the connection between at least two organs, using cardio-cerebral hemodynamics as a case study. Given the system's complexity, direct methods are unfeasible, so we use a scalable and robust algorithm based on the Newton-Krylov-Schwarz (NKS) framework [5], which has been successful in various single-organ systems [3], [6], [7]. While purely data-driven machine learning models offer advantages in simplified modeling requirements and near real-time computational efficiency [8], [9], physics-based approaches prioritize patient-specific anatomical and physiological uniqueness, avoiding dependence on extensive training datasets and emphasizing physical accuracy over generalized statistical correlations.

Translating computational results into clinical practice requires overcoming a critical barrier: traditional 2D screens limit spatial comprehension of multi-scale hemodynamic phenomena. Extended reality (XR) technologies—encompassing virtual, augmented, and mixed reality (VR/AR/MR)—address this gap by enabling immersive 3D visualization of patient-specific cardio-cerebral networks. Beyond visualization, XR enhances experimental interactivity and accuracy validation, allowing clinicians and researchers to manipulate and interrogate simulated environments directly, fostering deeper insights into complex physiological processes.

Recent advances demonstrate XR's potential in healthcare. VR-based platforms improve procedural proficiency in orthopedics [10], while studies by Sadeghi et al. [11] and Tsai et al. [12] illustrate XR's value in preprocedural planning for cardiovascular interventions. Sadri et al. [13] further extend this utility to cardio-cerebral hemodynamics modeling. Efforts to integrate computational modeling with XR are gaining momentum. Djukic et al.'s [14] VR-based fluid flow analysis simulations, Costagliola et al.'s [15] device-implantation frameworks, and Gong et al.'s [16] interactive digital heart. Wang et al. [17] developed advance surgical planning platforms, whereas Incekara et al. [18] and Qi et al. [19] leverage XR for neurosurgical navigation and functional brain mapping, respectively. The integration of XR in the study of cardio-cerebral hemodynamics holds great promise for advancing our knowledge in this field and improving the effectiveness of coronary revascularization procedures.

Despite its promise, the near real-time simulation of physical variables like velocity and pressure presents significant computational challenges. Achieving near real-time computation and real-time interaction requires pre-trained models for a near real-time computation and a real-time interaction. For surgeons, medical students, and other users, intuitive interfaces are essential to facilitate exploration without requiring in-depth knowledge of the algorithm and mesh details. Given the high computational cost of coupled systems, precomputed simulations are often necessary. This involves collecting patient-specific data and computing results for the original state, enabling rapid feedback during XR-guided interactions.

Remote collaboration among multiple users remains another critical challenge in XR-based medical applications. Over the past two decades, various groups have worked on this, including gesture-based VR guidance [20], shared gaze cues [21] and 3D panorama sharing [22], [23]. More recently, collaborative XR systems have begun integrating physiological data, such as in liver surgery planning [24], [25] and aortic interventions [17]. Building on this advancements, this paper propose a remote MR collaboration system for multi-organ hemodynamic analysis. By enabling geographically dispersed clinicians to interact with synchronized cardio-cerebral holograms in real-time. And also we show the interactive visualization.

The remainder of this paper is structured as follows. Section II details the architecture of the proposed remote collaborative diagnosis system, including its core components (the multi-organ model and the parallel method used for numerical simulation, and the visualization details) and the implementation of the remote collaboration and a real-time visualization. Section III presents experimental validation of this system, demonstrating its computational efficiency and accuracy. Finally, Section IV concludes with a discussion on the potential directions for future work.

II. Platform Architecture and Methodology

Figure 2 illustrates the core components of the proposed remote collaborative extended reality system, integrating three primary phases: offline numerical modeling, the near-real-time interaction, and remote collaboration. In this figure, the

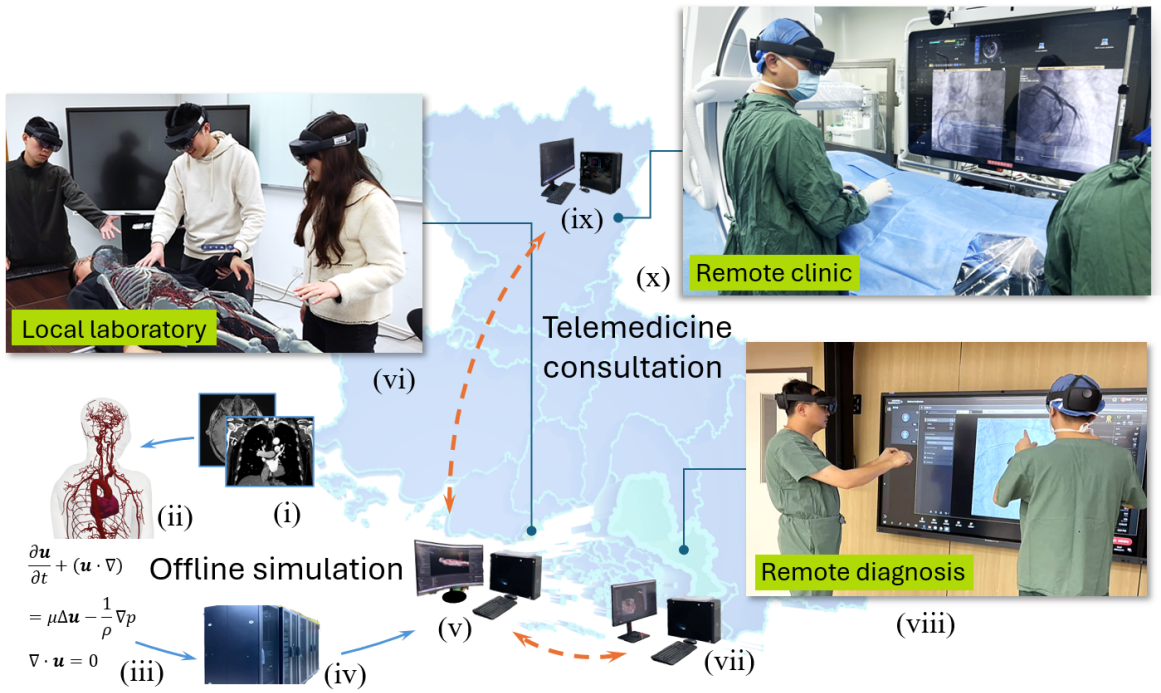

Fig. 2. Basic components of the remote collaborative extended reality system: (i)-(vi) local components: (i) patient-specific CT/MRI data; (ii) reconstructed cardiovascular geometry; (iii) mathematical model and the discretized data for simulation; (iv) parallel computer for simulation tasks; (v) local manager with GPU for data collection and visualization, connecting local and also remote managers; (vi) local collaborators. (vii)-(viii) remote components at place 1 for diagnosis: (vii) workstation at place 1, connected to the local manager; (viii) remote collaborators for diagnosis; (ix)-(x) remote components at place 2 for clinic: (ix) workstation at place 2, connected with local manager; (x) remote collaboration for clinic.

background depicts a map, with the workflow structure as follows:

1) Precomputed simulations: Located at the central hub ((i)-(vi) in Figure 2), this phase begins with the input of patient-specific data (e.g., MRI/CT scans) and mathematical models into a high-performance computing (HPC) cluster (Figure 2 (iv)). Foundational numerical simulations are carried out to generate the initial data.
2) Front-end visualization: The processed data from HPC is then transmitted to a local GPU workstation (Figure 2 (v)), facilitating rendering and translating the numerical results into interactive 3D visuals, along with providing near-real-time interaction feedback.
3) Remote collaboration setup: Figure 2 (vii)-(viii) are positioned at place 1, serving as as a diagnosis center, while Figure 2 (ix)-(x) are located at place 2, functioning as a clinic. These two geographically distant sites (Figure 2 (vii) and (ix)) are connected via a user datagram protocol (UDP) to synchronize interactions. Each site is equipped with head-mounted displays connected wirelessly, enabling clinicians to manipulate shared 3D hemodynamic models.

A. Numerical Modeling Preparation

The computational modeling workflow begins with patient-specific geometry reconstruction. For most MR technologies applied to the cardiovascular system, the integration of holographic images, derived from convectional imaging modalities, into real-world scenarios, particularly within surgical or procedural settings [26]. Various medical imaging techniques such as CT, MRI, echocardiography, and angiography have been employed in relevant studies. Among these techniques, CT stands out as the most commonly method for image acquisition, providing remarkable visualization of vascular structures and facilitating 3D reconstruction. Considering the soft tissues in brain, including gray matter, white matter, and cerebrospinal fluid, MRI's excellent soft-tissue contrast allows precise delineation of the complex network of cerebral blood vessels. In light of this, a hybrid imaging strategy is used for the cardio-cerebral arterial network, using MRI for cerebral imaging to capture their fine-scale details, while CT is used for the coronary arteries.

As illustrated in Figure 3, (i) and (ii) represent the raw imaging data, which processed to delineate the target vascular structures, as demonstrated in 3 (iii). Subsequently, Figure 3 (iv) shows the reconstructed cardio-cerebral arterial network. With the obtained 3D network, non-uniform meshes with varying local densities are created to cover the entire computational domain for numerical simulations, shown in Figure 3 (v), with detailed views of cerebral and coronary arteries presented in Figures 3 (vi) and (vii), respectively. The flowchart on the left side provides details of the segmentation

and reconstruction process, In cases where manual corrections do not meet the requirements, the segmentation part needs to be repeated. Moreover, during surface smoothing, if sharp angles appear, the reconstruction process will be reiterated. This entire process serves as preparatory groundwork for subsequent numerical simulations.

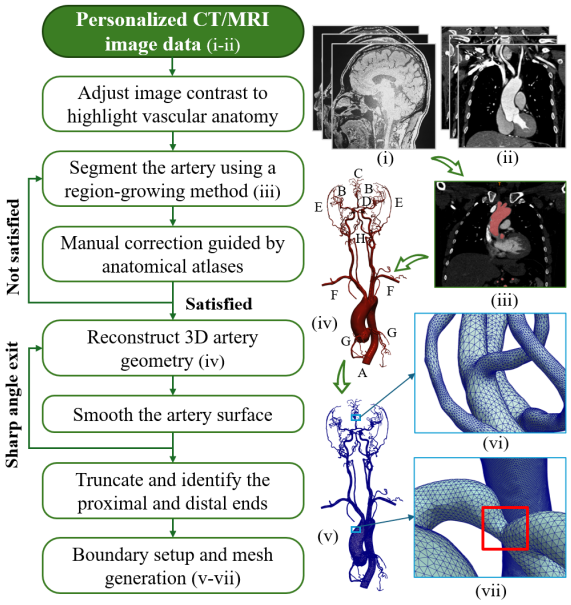

Fig. 3. Medical images unique to each patient are subjected to a segmentation and reconstruction process to generate a 3D representation of the arterial network.

1) Mathematical Modeling of Multi-Scale Hemodynamics: The human arterial network is represented as a composite domain $\Omega = \Omega_m \cup \sum_i \Omega_{s_i}$ (refer to Figure 1), where Ω_m denotes the major arteries, and Ω_{s_i}, with $i = 0, \ldots, n_s$, is the downstream vascular subnetworks in organs such as the liver and kidneys. Here, n_s is the number of organs involved. The topology of Ω dynamically adjusts to the focus in practical, resulting in varying inlet and outlet configurations for single-organ versus multi-organ analyses. As blood flow characteristics differ across the arterial network, tailoring models to these variations helps in capturing the true nature of blood movement within each artery type. Each artery segment has distinct inlet and outlet conditions that influence flow dynamics. Additionally, the interaction between arteries and downstream subnetworks in organs necessitates models that can effectively handle these interfaces and interdependencies.

We model the blood flow using the incompressible Navier-Stokes equations in network Ω:

$$\begin{cases} \rho\left(\dfrac{\partial \mathbf{u}}{\partial t} + (\mathbf{u}\cdot\nabla)\mathbf{u}\right) - \nabla\cdot\boldsymbol{\sigma} = \mathbf{0}, & \text{in } \Omega\times(0,T], \\ \nabla\cdot\mathbf{u} = 0, & \text{in } \Omega\times(0,T], \\ \mathbf{u}|_{t=0} = \mathbf{u}_0, & \text{in } \Omega, \end{cases} \tag{II.1}$$

where $\mathbf{u}$ is the velocity, ρ is the blood density, and $\boldsymbol{\sigma} = -p\mathbf{I} + \mu\left(\nabla\mathbf{u} + \nabla\mathbf{u}^T\right)$ is the Cauchy stress tensor, where $\mathbf{I}$ is an identity matrix, p is the blood pressure, and μ is the blood viscosity. T is the time period of a cardiac cycle. $\mathbf{u}_0$ is the initial condition for the velocity.

Let $\partial\Omega = \Gamma_I \cup \Gamma_W \cup \sum_j \Gamma_O^j$ be the boundary of the main network, with Γ_I, Γ_W, and Γ_O^j denoting the inlet, the wall, and the jth outlet boundaries. At Γ_I, we define the velocity profile of the blood entering the aorta based on cardiac output values $\mathbf{u} = \mathbf{v}(t)$, with a no-slip and no-penetration boundary condition $\mathbf{u} = \mathbf{0}$ at the impermeable, slip-free wall. To account for the resistant effect of the truncated downstream, we consider a three-element Windkessel model that leads to the following boundary condition at each outlet Γ_O^j,

$$\begin{aligned} p_j(t) \quad &= \left(p_j(0) - R_{1j}Q_j(0)\right)e^{-t/\tau_j} + \\ &R_{1j}Q_j(t) + \int_0^t \frac{e^{-(t-s)/\tau_j}}{C_j} Q_j(s)ds \\ &= \left(p_j(0) - R_{1j}\int_{\Gamma_O^j} \mathbf{u}(0)\cdot\mathbf{n}_O^j d\Gamma\right)e^{-t/\tau_j} + \\ &R_{1j}\int_{\Gamma_O^j} \mathbf{u}\cdot\mathbf{n}_O^j d\Gamma \\ &+ \int_0^t \left(\frac{e^{-(t-s)/\tau_j}}{C_j}\int_{\Gamma_O^j}\mathbf{u}(s)\cdot\mathbf{n}_O^j d\Gamma\right)ds, \end{aligned} \tag{II.2}$$

where $\tau_j = R_{2j}C_j$, $p_j(t)$ and $Q_j(t)$ are the pressure and the flow rate at the jth outlet, and $\mathbf{n}_O^j$ is the outward unit normal vector. $p_j^b(t)$ represents the distal pressure usually assumed to be 0. R_{1j} is the proximal resistance and R_{2j} and C_j are the resistance and compliance of the downstream vasculature. As it is unfeasible to acquire physiologically precise initial conditions $\mathbf{u}_0$, we generate them by initiating the simulation with zero velocity and pressure for a few time steps. The resultant initial conditions are found to be quite reasonable.

2) High-Performance Parallel Computing and Parameter Optimization: The governing equations are discretized into a large-scale sparse nonlinear algebraic system, and we consider a scalable Newton-Krylov-Schwarz (NKS) algorithm. An inexact Newton framework iteratively solves the nonlinear system, with Krylov subspace methods applied to the analytically derived Jacobian systems. To accelerate convergence, the restricted additive Schwarz method preconditioner is used, enhancing parallel scalability.

The computational domain Ω is divided into n subdomains $\{\Omega_i\}_{i=1}^n$ using graph-based decomposition tools (e.g., METIS/ParMETIS [27]), as shown in Figure 4. Each subdomain is designed to contain approximately the same number of elements to ensure computational load balance. The partitioning strategy aims to minimize interface sizes between subdomains, thereby reducing inter-process communication costs. Figure 4 visually depicts domain partitions and the overlaps between two adjacent subdomains, these overlaps can reduce the required iterations despite introducing marginal communication overhead. This trade-off enhances overall efficiency, as the computational gains from fewer iterations outweigh the increased synchronization costs. Each subdomain is assigned to a dedicated MPI process on a distinct processor core, where local matrix assembly and residual computations are performed independently. Interface solutions are harmo-

nized across processes via MPI point-to-point communication, enabling parallel resolution of the global system.

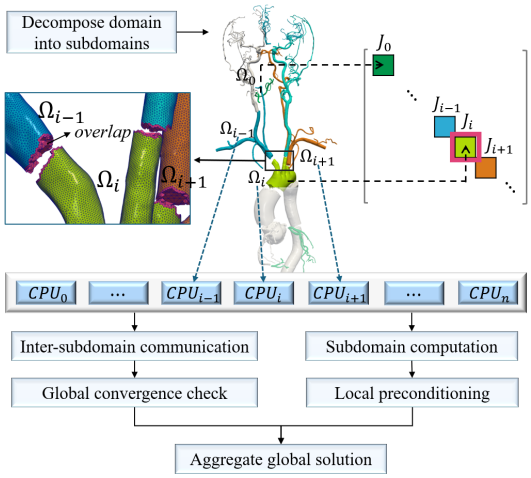

Fig. 4. Parallel computing workflow. The entire domain (problem) is decomposed into many subdomains (subproblems) that are assigned to different processor cores and solved in parallel.

B. Edge-Computing on Holographic-Devices

While traditional 2D screens are commonly used for displaying simulation results, they have significant limitations in terms of user interaction, immersive experience, and spatial comprehension, particularly when dealing with multi-scale systems. The reliance on keyboard and mouse inputs, along with restricted fields of view, can hinder intuitive interaction. Additionally, complex geometries like cardio-cerebral networks often exceed the spatial capabilities of conventional displays. To address these challenges, MR head-mounted displays offer a transformative alternative. By replacing traditional interfaces with natural interactions such as gesture tracking and voice commands [13], [28], MR enables clinicians to manipulate 3D holograms in an immersive, context-aware environment, fostering a deeper understanding of anatomy and enhancing spatial awareness.

In our framework, the desktop GPU acts as a computational bridge between high-performance computing resources and MR displays. This GPU serves as central hub for rendering high-quality 3D models, dynamic textures, and interactive hemodynamic visualizations. Once the numerical simulations are finished, the results are sent to the workstation for initial visualization. Subsequently, we use Unity [29] to configure the rendering results, which involves deploying them to appropriate locations and setting up specific commands, functions, and menus tailored to system's requirements. For example, the key functions in this study, the remote collaboration and real-time visualization of physical data. The final output is streamed wirelessly to the head-mounted displays via a shared Wi-Fi network, enabling real-time feedback and scene updates during collaborative analysis.

With the precomputed simulations for the initial data, when users modify vascular geometry (e.g., stent expansion or stenosis resection), only local mesh refinements are applied to the affected regions, preserving the majority of the pre-solved flow field. This localized adaptation strategy exploits the precomputed solution as a physics-informed preconditioner, significantly accelerating iterative convergence by initializing simulations from near optimal initial guesses. By minimizing global recomputation, the approach benefits computation efficiency.

C. Real-Time Interaction with Remote Users

Effective communication is crucial for collaborating with remote users located in various cities worldwide. This ensures seamless content sharing within the digital environment, which includes 3D models and results generated during front-end visualization, as well as synchronized operations of digital objects. To achieve this, we employ a host-client model to establish connections and share operations. The host initiates the connection, enabling multiple users to engage in collaboration from any location globally via the Internet. When the application starts on the host side, all objects are instantiated locally. Once clients connect to the host, they are instructed to create local copies of these objects without ownership, meaning only the host can control these objects. Synchronization processes are then initiated for these objects. The host can control the digital model, with their actions synchronized across all clients. Clients also have the option to request control of the digital model, with their commands first sent to the host and then broadcast to all other clients. This data is transmitted using the UDP, which offers lower latency and reduced overhead compared to the Transmission Control Protocol (TCP). Although UDP lacks guaranteed packet delivery or message order preservation, its low latency contributes to a smoother and more comfortable collaboration experience.

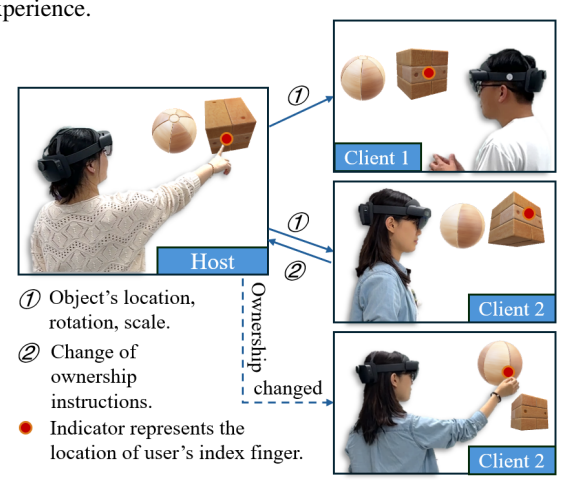

Fig. 5. A remote collaboration system featuring dynamic control transfer. Clients initially receive non-editable local replicas of shared objects and can observe the host's index finger movements in real time upon the host launching the application. Editing privileges are granted to a client only after an explicit request for control is made and approved.

Upon connection, an indicator representing the location of each user's index finger (depicted as a red ball in Figure 5),

including that of the host, is generated. This feature assists remote users in identifying the current focal points of all participants, thereby enhancing focus and coordination during collaborative activities. Although an indicator is generated for each user to show what they are focusing on, it can sometimes be difficult to locate due to the abundance of digital content. To address this, we have implemented another synchronization method that aligns the views of all users. When the digital world is created, each device establishes a local coordinate system with a common origin point in the digital realm. This ensures that the locations of all digital objects are consistent across all users, meaning the distances between these objects and their respective origin points are identical in the digital world, even though these origin points do not correspond to physical locations. The only variables are the position and rotation of the virtual camera, which represents the user's viewpoint in the digital world as they move and look around. This allows us to easily synchronize each user's view by adjusting the virtual camera's location to a specific shared position. In the physical world, users look at content through the lenses of their holographic glasses. However, in the digital world, it is the virtual camera that views the content displayed on these lenses. The coordinate system for the digital world is fixed by the glasses, regardless of the user's physical location. Therefore, to align each user's view, we only need to adjust the virtual camera's position in the digital world to be the same.

III. Experiments

In this section, we focus on a case study for the cardio-cerebral artery and discuss the system's capabilities for numerical modeling and remote diagnosis. We outline the mathematical model, discuss numerical simulation results and delve into the analysis of these outcomes using remote holographic collaboration.

A. Evaluation of Mathematical Model

As illustrated in Figure 3 (vii) (highlighted with red square), the patient exhibits significant stenosis with around 70% narrowing of the left main coronary artery. To simulate the effects of coronary artery revascularization, we replaced the narrowed segment with a standardized structure, replicating the deployment of a stent in clinical practice. Following established clinical sizing guidelines, the stenotic region (minimum diameter is 1.7mm) was expanded to a post-revascularization diameter of 4.65mm, effectively restoring the vessel to its natural dimensions. Modifications within the holographic interface involve adjusting mesh points or introducing a stent in the artery, these alternations are transmitted to the cluster for numerical simulations, with results subsequently returned to the workstation and displayed the head-mount displays for visualization.

The mathematical model we considered is represented by II.1, with a constant density of $\rho = 1.050\ g/cm^3$ and a viscosity of $\mu = 0.035\ cm^2/s$. Within the cardio-cerebral network, there are 118 outlets categorized into eight anatomical regions (refer to Figure 3 (iv) labeled A-H). These regions include the descending aorta, main cerebral artery, anterior cerebral artery, posterior cerebral artery, extracranial artery, subclavian artery, coronary artery, and others. Unique Windkessel parameters R_{2j} and C_j $(j = 1, \cdots, 8)$ are set for each group to effectively model them, as outlined in Table I. We use P1-P1 stabilized finite element method for the spatial discretization, while the temporal discretization use the second-order backward differentiation formula. The simulation covers one cardiac cycle, with a duration of $T = 1.0s$ and a time-step size of $\Delta t = 0.005s$. The stopping criteria for the NKS algorithm include relative residuals $\zeta \leq 1.0 \times 10^{-4}$ for linear solvers and $\epsilon \leq 1.0 \times 10^{-6}$ for nonlinear solvers. The overlapping size is 2 and the subdomain solver uses incomplete LU factorization with fill-ins set to 2. Additionally, a restart number of $k = 200$ is specified for the restart GMRES(k).

TABLE I
Information of different groups of outlets.

	A	B	C	D	E	F	G	H
Number of outlets	1	27	27	6	25	13	23	6
$R_j(dyness/cm^5)$	2164	22933	42167	62246	20424	8218	26143	93370
$C_j(cm^5/dyn)$	4.2e-4	4.0e-5	2.2e-5	1.5e-5	4.5e-5	9.8e-6	1.1e-4	3.5e-5

The pressure distribution pre- and post-revascularization are shown in Figure 6. In the traditional 2D screen (Figure 6 (a)), a notable increase in pressure is observed in the left stenotic area post-revascularization, indicating the effectiveness of the algorithm in restoring coronary artery perfusion. While the global numerical change slightly from [61.06, 106.92] mmHg to [61.38, 106.01] mmHg, suggesting a robust autoregulatory capacity within the circulation, these minor adjustments may obscure critical local flow redistribution. For example, discerning subtle differences in cerebral blood flow pre- and post-reconstruction solely based on color in the figure is challenging. However, a detailed data analysis tells that except the coronary artery, all outlets in the cerebral artery show a decreased in pressure and the mean volume flow rate. The

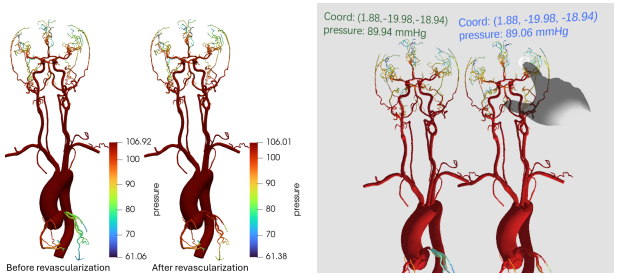

(a) Traditional screen-based visualization (b) Immersive head-mounted display

Fig. 6. Comparative visualization of coronary artery pressure distribution across pre- and post-revascularization states through traditional (a) and head-mounted display (b) modalities.

spatial resolution limitations of traditional 2D visualization make it challenging to identify statistically significant trends in low-variance regions. To address this issue, we use head-mount displays to enable 3D volumetric exploration, enhancing clinician's ability to detect critical spatial and temporal variations in multi-organ hemodynamics.

B. Visualization in MR Devices

Instead of directly transferring the colored objects to head-mount displays, our approach involves transferring visualization toolkit (VTK) [30] files which containing meshes and associated values to text files with special templates. This process allows interactive exploration of mesh information and value details through touch interaction. It key steps involving reading VTK files, extracting the mesh data and relevant field values, applying a color map for visualization, tracking the position of the user's right index finger via holographic sensors and displaying information when colliders for both the finger and the object intersect.

There are also two arteries in Figure 6 (b) which is captured from the MR devices, the left artery presents the pressure results pre-revascularization, while the right side presents post-revascularization data. We can first select a point on the left results then find the same point on the right one. A detailed comparative analysis at a specific point (1.88, -19.98, -18.94) reveals a pressure decrease from 89.94 mmHg to 89.06 mmHg in the cerebral pressure post-revascularization at that location.

Figure 7 demonstrates the system's ability in visualizing hemodynamic changes, extending beyond pressure analysis to critical velocity dynamics. The density and intricacy of streamlines effectively depict the fluctuations of velocity, with denser streamlines indicating higher velocities. And we also need to pay attention to the vortices within the streamline. By importing data rather than physical objects into MR devices, real-time generation of streamlines becomes feasible through the placement of the streamline tracer within head-mount displays. Subfigure (i) in Figure 7 illustrates that we can use interactive tools, such as a two-finger gesture, to measure the size changes pre-/post-revascularization of the geometry. Then, various streamline generation options are presented in Figure 7 (ii) including two most common approaches locating with point or lines. For example, we select point source and it leads to the appearance of a blue ball on the screen in Figure 7 (iii), which is a movable tracer that can be scaled and positioned at desired locations within the artery. As depicted in Figure 7, we put the ball within the artery and the streamlines at this place will be shown on the screen immediately, the color represents the value of velocity. Moreover, advanced functions also included to enhance the visualization of streamlines as shown in Figure 7 (v)-(vi), adjusting the length of the streamlines referred to as truncation, controlling the transparency of the streamlines, configuring the number of seed points in the streamline tracer and other features similar to ParaView. Figure 7 (vii) shows the streamlines in cerebral arteries, comparing to traditional 2D visualization tools, this system offers a more intuitive way for users to explore the details even a complex, coupled systems at different scales. This interactive paradigm shifts hemodynamic analysis from static observation to dynamic exploration, allowing clinicians to simulate blood flow abnormalities with greater precision.

IV. Summary

We present a MR-based remote diagnosis system for the assessment of cardiovascular disease, designed to quantify multi-organ hemodynamic interactions through patient-specific simulations and collaborative holographic visualization. The system integrates numerical modeling, physics-based simulations of patient-specific anatomies parallelized on supercomputers, with MR-guided interaction, enabling users to manipulate 3D holograms of cardiovascular networks via gestures while receiving near-real-time feedback from precomputed results. A practical case study demonstrates its ability to predict stroke risk during coronary revascularization. By simulating stent-induced geometric changes in coronary arteries, the system reveals how localized interventions affect cerebral blood flow, a risk traditionally overlooked in single-organ analyses. Users can dynamically adjust virtual parameters of the main arteries and visualize downstream hemodynamic responses, enabling data-driven optimization of surgical strategies. By integrating high-performance computing, multi-organ coupling, distributed MR collaboration, and the generation of streamlines in head-mounted displays, this framework propels precision cardiovascular care forward, offering comprehensive risk assessment and interactive planning capabilities that surpass traditional approaches.

References

[1] G. De Nisco, M. Lodi Rizzini, R. Verardi, C. Chiastra, A. Candreva, G. De Ferrari, F. D'Ascenzo, D. Gallo, and U. Morbiducci, "Modelling blood flow in coronary arteries: Newtonian or shear-thinning non-Newtonian rheology," *Computer Methods and Programs in Biomedicine*, vol. 242, p. 107823, 2023.

[2] J. G. Isaksen, Y. Bazilevs, T. Kvamsdal, Y. Zhang, J. H. Kaspersen, K. Waterloo, B. Romner, and T. Ingebrigtsen, "Determination of wall tension in cerebral artery aneurysms by numerical simulation," *Stroke*, vol. 39, no. 12, pp. 3172–3178, 2008.

[3] R. Chen, B. Wu, Z. Cheng, W.-S. Shiu, J. Liu, L. Liu, Y. Wang, X. Wang, and X.-C. Cai, "A parallel non-nested two-level domain decomposition method for simulating blood flows in cerebral artery of stroke patient," *International Journal for Numerical Methods in Biomedical Engineering*, vol. 36, no. 11, p. e3392, 2020.

[4] Z. Yan, D. Shang, R. Chen, J. Liu, and X.-C. Cai, "A computational study of the connection between coronary revascularization and cardio-cerebral hemodynamics," *Computer Methods and Programs in Biomedicine*, vol. 263, p. 108667, 2025.

[5] L. Luo, X.-C. Cai, Z. Yan, L. Xu, and D. E. Keyes, "A multilayer nonlinear elimination preconditioned inexact Newton method for steady-state incompressible flow problems in three dimensions," *SIAM Journal on Scientific Computing*, vol. 42, no. 6, pp. B1404–B1428, 2020.

[6] Z. Lin, R. Chen, B. Gao, S. Qin, B. Wu, J. Liu, and X.-C. Cai, "A highly parallel simulation of patient-specific hepatic flows," *International Journal for Numerical Methods in Biomedical Engineering*, vol. 37, no. 6, p. e3451, 2021.

[7] S. Qin, R. Chen, B. Wu, and X.-C. Cai, "A highly parallel fully implicit domain decomposition method for the simulation of the hemodynamics of a patient-specific artery at the full-body scale," *Journal of Computational Physics*, vol. 472, p. 111730, 2023.

[8] C. Kulkarni, A. Quraishi, M. Raparthi, M. Shabaz, M. A. Khan, R. A. Varma, I. Keshta, M. Soni, and H. Byeon, "Hybrid disease prediction approach leveraging digital twin and metaverse technologies for health consumer," *BMC Medical Informatics and Decision Making*, vol. 24, no. 1, p. 92, 2024.

[9] Z. Rudnicka, K. Proniewska, M. Perkins, and A. Pregowska, "Cardiac healthcare digital twins supported by artificial intelligence-based algorithms and extended reality-a systematic review," *Electronics*, vol. 13, no. 5, 2024.

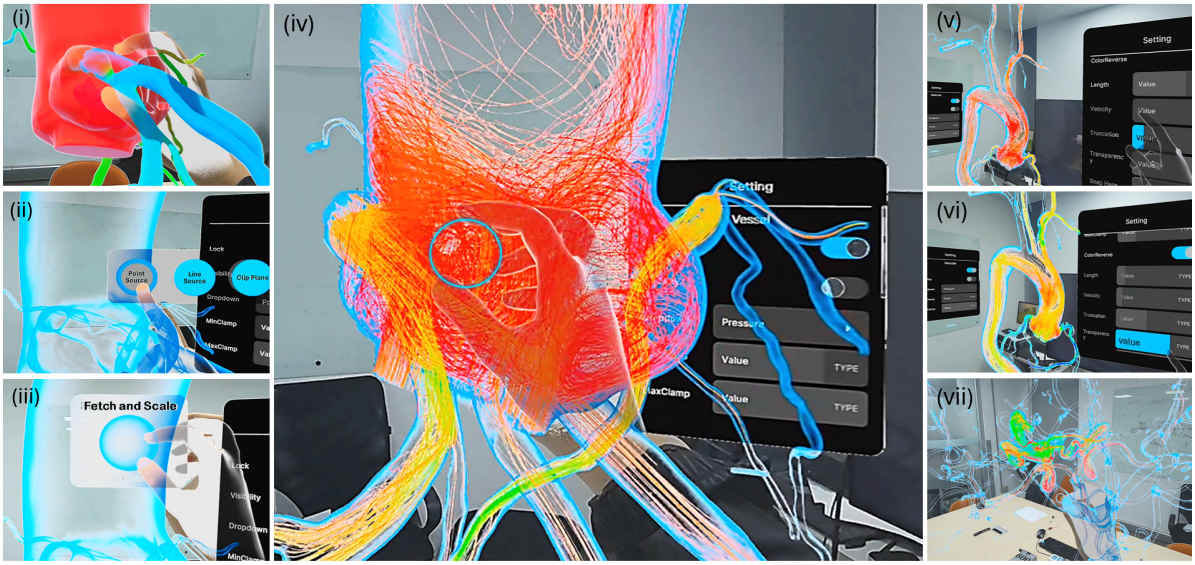

Fig. 7. MR-guided hemodynamic exploration: (i) the comparison of pre-/post-revascularization in pressure and geometry; (ii) the approaches for generating streamlines; (iii) a movable point-source tracer; (iv) localized streamlines at the marked point in blue; (v) a slider to adjust the length of the streamlines; (vi) a transparency controller; and (vii) the streamlines in cerebral artery.

[10] J. T. Verhey, J. M. Haglin, E. M. Verhey, and D. E. Hartigan, "Virtual, augmented, and mixed reality applications in orthopedic surgery," *The International Journal of Medical Robotics and Computer Assisted Surgery*, vol. 16, no. 2, p. e2067, 2020.

[11] A. H. Sadeghi, S. El Mathari, D. Abjigitova, A. P. Maat, Y. J. Taverne, A. J. Bogers, and E. A. Mahtab, "Current and future applications of virtual, augmented, and mixed reality in cardiothoracic surgery," *The Annals of Thoracic Surgery*, vol. 113, no. 2, pp. 681–691, 2022.

[12] T.-Y. Tsai, Y. Onuma, A. Złahoda-Huzior, S. Kageyama, D. Dudek, Q. Wang, R. P. Lim, S. Garg, E. K. W. Poon, J. Puskas, F. Ramponi, C. Jung, F. Sharif, A. A. Khokhar, and P. W. Serruys, "Merging virtual and physical experiences: extended realities in cardiovascular medicine," *European Heart Journal*, vol. 44, no. 35, pp. 3311–3322, 2023.

[13] S. Sadri, G. J. Loeb, A. Grinshpoon, C. Elvezio, S. H. Sun, V. G. Ng, O. Khalique, J. W. Moses, A. J. Einstein, A. J. Patel, I. George, R. T. Hahn, T. M. Nazif, M. B. Leon, A. J. Kirtane, S. K. Kodali, S. K. Feiner, and T. P. Vahl, "First experience with augmented reality guidance for cerebral embolic protection during TAVR," *JACC: Advances*, vol. 3, no. 3, p. 100839, 2024.

[14] T. Djukic, V. Mandic, and N. Filipovic, "Virtual reality aided visualization of fluid flow simulations with application in medical education and diagnostics," *Computers in Biology and Medicine*, vol. 43, no. 12, pp. 2046–2052, 2013.

[15] E. Costagliola, F. Musumeci, C. Gandolfo, M. Pilato, and S. Pasta, "Merging mixed reality and computational modeling for enhanced visualization of cardiac biomechanics," *Medical Engineering and Physics*, vol. 134, p. 104258, 2024.

[16] Y. Gong, F. Qi, J.-Y. Wang, Y. Liu, T. Ma, Z. Cheng, Y. Jiang, R. Chen, X. Wang, L. Luo, and X.-C. Cai, "An interactive platform for a high performance digital twin of a human heart," in *2023 IEEE International Conference on Metaverse Computing, Networking and Applications (MetaCom)*, 2023, pp. 193–200.

[17] J.-Y. Wang, Y. Gong, J. Zhou, F. Qi, Y. Liu, Z. Cheng, R. Chen, X. Wang, L. Luo, and X.-C. Cai, "A collaborative mixed reality platform for the planning of vascular surgery," in *2024 IEEE International Conference on Metaverse Computing, Networking, and Applications (MetaCom)*, 2024, pp. 9–16.

[18] F. Incekara, M. Smits, C. Dirven, and A. Vincent, "Clinical feasibility of a wearable mixed-reality device in neurosurgery," *World Neurosurgery*, vol. 118, pp. e422–e427, 2018.

[19] F. Qi, Y. Liu, Y. Gong, J.-Y. Wang, J. Zhou, R. Chen, R.-S. Huang, X. Wang, L. Luo, and X.-C. Cai, "Mixed reality visualization and interactive hemodynamic computation of the human brain," in *2024 IEEE International Conference on Metaverse Computing, Networking, and Applications (MetaCom)*, 2024, pp. 17–24.

[20] W. Huang, L. Alem, F. Tecchia, and H. B.-L. Duh, "Augmented 3D hands: a gesture-based mixed reality system for distributed collaboration," *Journal on Multimodal User Interfaces*, vol. 12, no. 2, pp. 77–89, 2018.

[21] J. Shin, G. Suh, S.-H. Kim, H.-J. Yang, J.-E. Shin, G. Lee, and S. Kim, "Effect of the hand and gaze pointers in remote collaboration," *IEEE Access*, vol. 12, pp. 172 774–172 784, 2024.

[22] H. Bai, P. Sasikumar, J. Yang, and M. Billinghurst, "A user study on mixed reality remote collaboration with eye gaze and hand gesture sharing," in *Proceedings of the 2020 CHI Conference on Human Factors in Computing Systems*. New York, NY, USA: Association for Computing Machinery, 2020, p. 1–13.

[23] X. Zhang, X. Bai, S. Zhang, W. He, P. Wang, Z. Wang, Y. Yan, and Q. Yu, "Real-time 3D video-based MR remote collaboration using gesture cues and virtual replicas," *The International Journal of Advanced Manufacturing Technology*, vol. 121, no. 11, pp. 7697–7719, 2022.

[24] V. Chheang, P. Saalfeld, F. Joeres, C. Boedecker, T. Huber, F. Huettl, H. Lang, B. Preim, and C. Hansen, "A collaborative virtual reality environment for liver surgery planning," *Computers & Graphics*, vol. 99, pp. 234–246, 2021.

[25] V. Chheang, D. Schott, P. Saalfeld, L. Vradelis, T. Huber, F. Huettl, H. Lang, B. Preim, and C. Hansen, "Advanced liver surgery training in collaborative VR environments," *Computers & Graphics*, vol. 119, p. 103879, 2024.

[26] I. T. Moon, S.-K. Ko, S.-H. Kang, C.-H. Yoon, T.-J. Youn, and I.-H. Chae, "Augmented reality in cardiology: Enhancing visualization and precision," *Current Cardiovascular Risk Reports*, vol. 18, no. 12, pp. 175–186, 2024.

[27] K. Schloegel, G. Karypis, and V. Kumar, "Parallel multilevel algorithms for multi-constraint graph partitioning," in *Euro-Par 2000 Parallel Processing*, A. Bode, T. Ludwig, W. Karl, and R. Wismüller, Eds. Berlin, Heidelberg: Springer Berlin Heidelberg, 2000, pp. 296–310.

[28] J. Liu, S. J. Al'Aref, G. Singh, A. Caprio, A. A. A. Moghadam, S.-J. Jang, S. C. Wong, J. K. Min, S. Dunham, and B. Mosadegh, "An augmented reality system for image guidance of transcatheter procedures for structural heart disease," *PLOS ONE*, vol. 14, no. 7, pp. 1–16, 2019.

[29] Unity Technologies, "Unity," 2023. [Online]. Available: https://unity.com

[30] W. Schroeder, K. Martin, and B. Lorensen, *The Visualization Toolkit (4th ed.)*. Kitware, 2006.